ELSEVIER

Geoderma 108 (2002) 237–257

GEODERMA

www.elsevier.com/locate/geoderma

Microscale investigation into the geochemistry of arsenic, selenium, and iron in soil developed in pyritic shale materials

Daniel Strawn [a,*], Harvey Doner [b], Mavrik Zavarin [c], Scott McHugo [d]

[a] *University of Idaho, Moscow, ID, USA*
[b] *University of California-Berkeley, Berkeley, CA, USA*
[c] *Lawrence Livermore National Laboratory, Livermore, CA, USA*
[d] *Lawrence Berkeley National Laboratory, Berkeley, CA, USA*

Received 28 May 2001; received in revised form 22 January 2002; accepted 14 February 2002

Abstract

In this study, we report on the distribution and mineralogy of micron-sized mineral aggregates formed in the top horizon of an acid sulfate soil. The distribution and oxidation state of arsenic (As) and selenium (Se) were also determined. The soil used in this study was formed from pyritic shale parent materials on the east side of the California Coast Range. Synchrotron-based X-ray fluorescence microprobe (μ-XRF) was used to generate elemental distribution maps of soil thin sections. Using the elemental distribution maps and optical micrographs, distinct mineral aggregates of iron oxide and iron sulfate were identified throughout the top horizon of the soil. These aggregates range in size from 10 to 100 μm in diameter and can be found only a few micrometers apart. The As and Se concentrations in the iron oxide aggregates were 5–10 times the concentrations in the iron sulfate aggregates and the weathered shale matrix. This suggests that the As and Se become preferentially associated with iron oxides during the weathering process. Using a focused micron-sized beam, Fe, As, and Se X-ray absorption spectroscopy (XAS) data were collected from the sub-millimeter soil aggregates. The micro-extended X-ray absorption fine structure (μ-EXAFS) spectrum collected from the iron oxide aggregate revealed that its mineralogy was a combination of ferrihydrite (>50%) and goethite. The μ-EXAFS spectra from the iron sulfate region suggest that these aggregates contain jarosite. Using micro-X-ray absorption near edge spectroscopy (μ-XANES), oxidation states of the As and Se were determined. Arsenic was present in the iron oxide aggregate as As(V). Selenium was present in the soil as both Se(IV) and Se(VI), with a higher percentage of Se(VI) in the jarosite aggregate than the iron oxide aggregate. These results provide direct evidence of the distribution, oxidation states, and speciation of As and Se in the solid phase of an unaltered

* Corresponding author. University of Idaho, Moscow, ID, USA. Fax: +1-208-885-7760.
E-mail address: dgstrawn@uidaho.edu (D. Strawn).

PII: S0016-7061(02)00133-7

native soil. Information on the weathering and geochemistry of the pyritic materials, and the associated arsenic and selenium is useful for predicting the pedogenic processes of acid sulfate soils and the long-term fate of newly exposed pyritic materials (e.g., mine tailings and drained wetlands).

Keywords: Micro-XAFS; Arsenic; Selenium; Iron minerals; Acid sulfate soils

1. Introduction

Reduced iron sulfur containing earth materials such as pyrite are significant sources of arsenic and selenium in the environment (Foster et al., 1998; Ganje and Rains, 1982; Masschelyn et al., 1991; Presser and Swain, 1990; Savage et al., 2000; Tamaki and Frankenberger, 1992; Velinsky and Cutter, 1990). In addition, the geochemistry of soils derived from pyritic parent materials are strongly influenced by the iron and sulfur weathering products (Lumsdon et al., 2001). Human activities such as mining, groundwater drawdown, and wetland drainage have exposed pyritic materials to a more oxidizing environment. The weathering of these newly exposed geological materials will oxidize and dissolve the reduced iron sulfur minerals, which will reprecipitate as secondary minerals. Two common minerals that result from the weathering of pyritic materials are iron oxides (e.g., goethite and ferrihydrite) and iron sulfates (jarosite) (Dudas et al., 1988; Evangelou and Zhang, 1995; Lumsdon et al., 2001). In semiarid or arid regions, sulfate salts such as gypsum and sodium sulfate may also be present in pyrite-influenced soils. As the pyrites weather, coprecipitated As and Se also undergo oxidation, forming new minerals or leaching out of the soils. The changes in the As and Se speciation affect the availability of these elements for transport into surface and ground waters, and uptake by plants and other biota. Thus, in order to better predict and model the fate of As and Se from Fe–S-rich materials, it is necessary to have a clear understanding of the geochemical processes that affect their oxidation state and mineral associations.

Soils whose geochemical properties are controlled by the oxidation of iron and sulfur minerals, in particular pyrite, are called acid sulfate soils (Fanning and Fanning, 1989). Some of the characteristics of these soils include, low pH, the presence of jarosite and sulfate salts, and extensive mottling due to iron oxide and sulfate mineral aggregates (Fanning and Fanning, 1989; Sencindiver and Ammons, 2000). These soils are commonly formed on sedimentary rocks of marine origin (e.g., shales). Mermut et al. (1985) studied the micromorphology and distribution of features related to pyrite oxidation in a soil derived from marine shale parent materials in Saskatchewan using scanning and transmission electron microscopes (SEM and TEM, respectively) and energy dispersive analysis of X-ray (EDX). Based on the shapes of the jarosite aggregates, Mermut et al. (1985) hypothesized that the jarosite was crystallized from the solution phase as opposed to in situ replacement of the pyrite phase. They found that the jarosite aggregates were most common in the lower horizons, while iron oxides were more common in the upper horizons. In the upper horizon, the iron minerals were identified as goethite and hematite based on crystalline morphology, while in the lower horizon, noncrystalline ferric

hydroxides were identified. Several other researchers have also studied the distribution and speciation of minerals in acid sulfate soils (Dudas et al., 1988; Fanning and Fanning, 1989; McSweeney and Madison, 1988; Ross et al., 1988; Sencindiver and Ammons, 2000).

Arsenic and Se occur in the environment in several oxidation states. The most common oxidation states of As in soils are three and five, while Se primarily occurs as four and six. More reduced forms of As and Se can occur in anoxic soils. During the formation of pyrite in reducing environments, As and Se are isomorphically substituted for reduced sulfur in the pyrite structure (Nesbitt et al., 1995; Presser and Swain, 1990). The oxidized forms of these elements exist in soils and solutions as the oxyanions arsenate (AsO_4^{3-}), arsenite (AsO_3^{3-}), selenate (SeO_4^{2-}), and selenite (SeO_3^{2-}). Lumsdon et al. (2001) modeled the weathering of an arsenopyrite/pyrite particle in water using thermodynamic data and a diffusion model. Their results showed a succession of As solubilization as the particle weathered; upon initial dissolution, dissolved As concentrations were at maximum, followed by a decrease as the pyrite weathered to jarosite, and the lowest dissolved As concentration occurring during the later stages of weathering when poorly ordered iron oxides were formed. A major reaction mechanism controlling the fate of As and Se in soils is sorption and desorption. The oxyanions are strongly sorbed as inner-sphere complexes on the functional groups of iron minerals (Fendorf et al., 1997; Fuller et al., 1993; Manceau and Charlet, 1994; Manning et al., 1998; O'Reilly et al., 2001). The extent of sorption of these oxyanions is dependent on pH. Although arsenate is thought to be the least mobile form of As, recent data has shown that at high concentrations or pH arsenite loading levels are higher than arsenate loading levels (Manning and Goldberg, 1997; Raven et al., 1998; Sun and Doner, 1998). Selenate is adsorbed less strongly than selenite, and is considered to be the most readily available species for bio-uptake and transport to surface and ground waters (Zhang et al., 1999).

The chemical speciation and physical distribution of As in both pyritic acid sulfate soils and mine spoils have been studied. Savage et al. (2000) and Foster et al. (1998) studied the oxidation state, molecular structure, and micromorphology of As from mine spoils located in California using X-ray absorption spectroscopy (XAS), X-ray diffraction (XRD), TEM, and SEM. They found that the weathering of arsenopyrite minerals released arsenate that either coprecipitated with iron sulfate and iron oxide minerals, or adsorbed on the surface of iron oxide or silicate minerals. Arsenate coprecipitates such as scorodite ($FeAsO_4$) have been observed in natural systems. Several studies have been done on the geochemistry of contaminants in mine tailings (Evangelou and Zhang, 1995; Fennemore et al., 1998; Foster et al., 1998; Ribet et al., 1994; Savage et al., 2000). However, few have evaluated trace element geochemical processes in naturally developing soils (i.e., basic pedogenic process), which is valuable for predicting the long-term fate of the trace elements (McSweeney and Madison, 1988; Sencindiver and Ammons, 2000). Dudas et al. (1988) evaluated the geochemistry of As in acid sulfate soils from Alberta using a sequential extraction technique and a thermodynamic chemical speciation program. They found that the As accumulated in pockets and veins of soil enriched in iron oxides and that calcium, manganese, and iron arsenate minerals were not thermodynamically stable. However, their results did not provide direct information about the microdistribution and oxidation state of As in the solid phase.

The geochemistry of Se mineral weathering mirrors that of S. In most oxidizing environments, Se exists primarily sorbed onto the surfaces of oxide minerals (Glasauer et al., 1995; Presser and Swain, 1990; Sposito et al., 1988). Most selenite and selenate minerals are too soluble to persist in natural environments (Masschelyn et al., 1991). However, some iron selenite minerals have been reported in acid environments, such as the insoluble ferric selenite ($Fe_2(OH)_4SeO_3$) (Presser and Swain, 1990), and selenate has been observed to be isomorphically substituted for sulfate in hydrous Mg and Na sulfate salts (Presser and Swain, 1990). In arid regions, sulfate salts with coprecipitated Se are common. Very little research has been done on the mineralogy of Se weathered from pyritic materials.

The objective of this study is to provide a better understanding of the natural geochemical cycling of arsenic and selenium in soils. To accomplish this objective, we utilized a new research tool that combines synchrotron-based micro-X-ray fluorescence (μ-XRF) spectroscopy and spatially resolved X-ray absorption fine structure spectroscopy (μ-XAFS). These tools are ideally suited for investigating micromorphology and chemical speciation in heterogeneous samples such as soils. By scanning across the surface with a focused X-ray beam, the elemental composition and spatial distribution of the elements can be determined. Utilization of the intense X-ray beams from a synchrotron source allows for the detection of elements present at much lower levels than is possible using an electron microscope (e.g., SEM). Since the spatial resolution of the synchrotron X-ray beam is ~ 1 μm, it is possible to focus on individual aggregates and particles and collect μ-XAFS spectra, which allows for determination of oxidation state and molecular structure of these microscopic features. Several researchers have used microscopic X-ray absorption near edge structure (μ-XANES) spectroscopy to determine the oxidation state of metals in natural samples (Bertsch et al., 1994; Tokunaga et al., 1997, 1998, and others); Manceau et al. (2000) and Alexander (1995) provided a review of this literature. However, only a few studies have used spatially resolved extended XAFS (μ-EXAFS) spectra from whole soils with their morphology intact (Manceau et al., 2000). EXAFS spectra provide detailed information on the local atomic structure surrounding the atom of interest (Fendorf and Sparks, 1996). In powder, EXAFS spectroscopy of heterogeneous samples deciphering the spectra is complicated by the presence of several different mineral phases, and no information on the morphology or spatial distribution can be obtained. Manceau et al. (2000) used μ-EXAFS to determine the chemical speciation of Zn in a whole soil collected near a smelter in France. They found that the Zn was present in the soil incorporated into phyllosilicates, and Mn and Fe oxide minerals. In the current study, μ-EXAFS spectroscopy is used to investigate the iron mineralogy of sub-millimeter aggregates in undisturbed soil cores, and μ-XANES is used to determine the oxidation state of As and Se in the soil aggregates.

The soil used in this study was collected from the east side of the California Coast Range. The soil has undergone natural pedogenic processes with only minor influences from range cattle. The parent materials for the soil are shale materials that contain small inclusions of pyrite. Eroded materials from these upland soils provide the parent materials for the alluvial soils of the Western San Joaquin Valley, which are extensively used for agriculture (Presser and Swain, 1990). Also, since these soils are formed on As and Se containing pyritic shale parent materials, the information gained from this study will be

important for evaluating the weathering and geochemistry of trace elements from other newly exposed pyrite containing materials over long time periods. Such information will lead to the development of effective management strategies for these soils.

2. Research procedures

2.1. Site description

Soil samples were collected from the top (A) horizon of a soil located in the Panoche Hills on the east side of the California Coast Range. This soil belongs to the Gewter series and is classified as a Ultic Haploxeralf (National Cooperative Soil Survey, 1997). The location of the study site is N36°35′ 32″, W120°41′ 28″. The slope at this site faces southeast and has an incline of 15%. The parent material for the soil is the Late Cretaceous to Paleocene Moreno formation (Presser and Ohlendorf, 1987). The Moreno formation consists of black shale containing small inclusions of pyrite. The A horizon is 2–4 cm deep, has small roots from annual grasses and forbs, and has a texture class of clay with 25% rock fragments consisting of soft friable shale material. The soils have a relatively high salt content as indicated by an electrical conductivity of 1.2 dS m^{-1} and the presence of evaporites in the cracks and crevices below 3 cm. Salt crystals were not observed in the sample used in this study. The vegetation on these soils is sparse, with some annual grasses and other forbs that have high salt tolerances. The pH of a 1:1 (soil/deionized water) gravimetric suspension of the soil was 4.0. This low pH is due to the formation of sulfuric acid from the oxidation of the pyritic mineral inclusions in the shale materials (sulfurication) (Fanning and Fanning, 1989).

2.2. Sample preparation

In April 1999, soils were collected using a soil-coring device (diameter = 4.5 cm) fitted with a Lucite sleeve that was capped after collection to preserve the morphology and aggregate distribution of the sample. The soil cores were air-dried at 35 °C, impregnated with LR White resin (SPI Supplies, West Chester, PA) under a vacuum and then cured in an oven at 60 °C for 24–48 h to induce resin hardening. The impregnated soil cores were cut into 2 × 3 × 0.3 cm pieces using a diamond-edged saw, after which they were ground to various thicknesses (0.5–3 mm). This preparation procedure results in small self-supporting wafers with morphologies intact that are flat enough so that the plane of focus is constant throughout the *xy* scan. Experiments on untreated soil material (see discussion below) showed no impacts on the oxidation state of Se from sample preparation. The data presented in this paper represent only a few isolated regions (on the order of 1 mm^2) and features from the soil. Soils have infinite variability, and cannot be completely characterized by a single 1 mm^2. However, microspectropic analysis was carried out on several regions and thin sections using three different beamline configurations (see below), and the results from all of the analyses were identical to those presented in this paper. Thus, it is inferred that the results discussed in this paper are applicable for the entire A horizon of the soil.

2.3. Microspectroscopic analysis

To determine the elemental distribution in soil thin sections, the samples were analyzed using a synchrotron-based X-ray fluorescence microprobe on beamline 10.3.1 at the Advanced Light Source (ALS), Lawrence Berkeley National Laboratory (Berkeley, CA). The storage ring at the ALS is operated at 1.9 GeV with a maximum current of 400 mA. Beamline 10.3.1 has an Si (Li) energy dispersive solid-state detector mounted at 90° incident to the X-ray beam, and Kirpatrick–Baez optical geometry to focus the monochromatic light to ~ 1 μm. The sample was held at a 45° angle and ~ 3 mm at closest point to the detector. The sample was scanned at an energy of 12.5 eV using an automatically controlled sample stage that rasters across the sample at predefined step sizes. Data were collected in 10-μm steps at 4 s per step. The final spectra were corrected for background and normalized to National Institute of Standards and Technology fluorescence spectroscopy standards that have known elemental concentrations (SRM 1832 and 1833). The units of the data are $\mu g/cm^2$, and allow for relative comparisons only. The Mn $K_{\beta 1}$ (6.490 keV) may contribute to the intensity of the Fe $K_{\alpha 1}$ peak, causing a small amount of error in the element concentrations. Converting from $\mu g/cm^2$ to μg/g soil in heterogeneous samples such as soils is difficult since the depth of penetration of the X-rays is dependent on the elemental composition, mineral density, and the fluorescence energy of the element being detected. Zavarin (1999) has discussed these limitations in detail, and has proposed some strategies for overcoming them. In this study, the variable X-ray penetration depth may have some impact on spatial resolution and relative elemental concentrations. However, scans from several samples yielded the same trends, indicating that the errors introduced from sample heterogeneity do not impact interpretation of the relative elemental distributions in the soil thin sections. Data were mapped using the contour-mapping feature available in the program Microcal Origin (North Hampton, MA).

The As (K edge) XANES and Fe (K edge) EXAFS spectra were collected on Beamline 10.3.2 at the ALS, and the Se (K edge) XANES spectra were collected at Beamline 13-ID-C at the Advanced Photon Source (APS), Argonne National Laboratory (Chicago, IL). Beamline 10.3.2 at the ALS uses elliptically bent mirrors to focus the beam to 1–5 μm with an Si(111) crystal to obtain monochromatic light (MacDowell et al., 1998). The detector at beamline 10.3.2 is an Si (Li) solid-state detector orientated at a 45° angle to the sample (90° incident to the beam), and can be moved in as close as 1 mm from the sample. Beamline 13-ID-C uses a Kirpatrick–Baez optical geometry to focus the monochromatic light obtained from an Si crystal monochromator to 1–5 μm. The detector used on BL 13-ID-C was a 13-element germanium detector with a 100-μm aluminum foil filter to prevent saturation of the detector electronics from the high Fe K edge fluorescence.

XANES data were collected using 0.4 or 0.5 eV steps at 0.5 to 15 s per step from ~ 1 μm spots in the sample. For Se XANES, the spectra from 8 to 10 channels were merged. For the As XANES, the spectra from 10 to 20 individual scans were merged. The scans were collected from 100 to 50 eV before the edge to 200 eV after the edge. The spectra were processed by subtracting pre-edge and post-edge backgrounds, and normalizing the step height to one. To test for the effects of resin impregnation on the As oxidation state,

soil cores were spiked with As(III) (final As loading = 781 mg (kg soil)$^{-1}$, equilibrium pH = 4.5) and prepared into thin sections as described above. To test for the effects of resin impregnation on the Se oxidation state, small jarosite aggregates were isolated from the unaltered soil under a dissecting microscope and the XANES spectra from these aggregates were compared to the XANES spectra from the impregnated samples. The possibility of beamline oxidation/reduction was evaluated by collecting several successive scans; the spectra showed no change over time. Arsenic and Se standard XANES data were collected from sodium arsenate, arsenite, selenite, and selenate salts dissolved in deionized water (0.1–0.001 M) and placed on a 0.2-μm polyethersulfone filter paper and sealed in Kapton. For the Se spectra, the salts were also run as solids diluted in boron nitride.

The iron μ-EXAFS spectra were collected on Beamline 10.3.2 at the ALS. Data acquisition of the Fe K edge (7.112 keV) was done by scanning from 200 eV before to 800 eV after the edge. The time for each scan was ~ 30 min. Multiple (15–25) scans were merged to increase the signal to noise ratio. Data reduction of the EXAFS spectra involved background subtraction, normalization, conversion to *k*-space, and weighting by k^3. All spectra (samples and standards) were processed using identical *k*-space, normalization, and background subtraction. The parameters were optimized by minimizing oscillations in the spline derivative, minimization of low R peak height in the radial structure function, and maximizing the peak height of the O backscatterer while minimizing its FWHM. Processing all of the spectra using the same parameters allows for relative comparisons between the spectra and the standards. The sample used for the Fe EXAFS data collection was a 0.5-mm-thick soil thin section. The standards used for fitting were well-characterized hematite, ferrihydrite, goethite, and jarosite minerals (Scheinost and Schwertman, 1999). The EXAFS spectra of the standards were collected in transmission using bulk EXAFS techniques.

Fitting of the EXAFS spectra was accomplished using a linear combination least squares optimization routine in the program WinXAFS. A similar approach for fitting EXAFS spectra was used by Manceau et al. (1996, 2000) and Gaillard et al. (2001). To begin the fitting process, the unknown chi spectrum was fitted using four iron mineral standard spectra (goethite, ferrihydrite, hematite, and jarosite). Standards that had partial contributions that were very low (< 1%) or negative were removed from the succeeding fits. The fit of the components were normalized so that they comprised 100% of the spectra from the aggregates. The final fit was taken as the fit that consisted of the least number of components and yielded the lowest residual. Manceau et al. (2000) reported that the accuracy of fitting EXAFS spectra linear combinations of standards is 15%; however, in our experiments, the error is higher since the EXAFS spectra from the samples were collected in fluorescence mode, while the EXAFS spectra from the standards were collected in transmission mode; self-absorption decreases the signal of the EXAFS spectra collected in fluorescence mode. We did not do any corrections for self-absorption since our samples have variable density, particle size, and elemental compositions; thus, our results are only semiquantitative. Attempts to fit the spectra from ab initio theoretical phase shifts and amplitudes was not attempted since the spectra terminate at ~ 10 Å^{-1}, and isolation and distinction of the backscattering shells would be difficult without more data.

3. Results and discussion

3.1. Identification of iron minerals using μ-EXAFS

Fig. 1 shows an optical image taken from a soil thin section. There were three unique features that were identified from this image: orange aggregates (medium tone gray in black and white micrograph, features labeled A), yellow aggregates (bright white in black and white micrograph, feature labeled B), and the brown matrix that is indicative of the shale parent material. These features were observed throughout the soil horizon. Previous X-ray diffraction (XRD) analysis of large bulk separates that were collected from nearby soils indicated that the orange materials are composed of primarily goethite, and the yellow separates are composed of jarosite (Zavarin, 1999). Small amounts of montmorillonite, illite, quartz, and muscovite were also identified in the separates. In the top soil horizon investigated in this study, the iron oxide and iron sulfur aggregates ranged in size from 10 to 100 μm, and are located within a few microns of each other. While XRD and color associations allow for some mineral identification, these techniques have limited use in determining mineralogy of poorly crystalline materials and heterogeneous samples, both common characteristics of soils (Schwertmann and Taylor, 1989). Since poorly crystalline iron oxides have highly reactive surfaces, it is important to include them in mineralogical characterization.

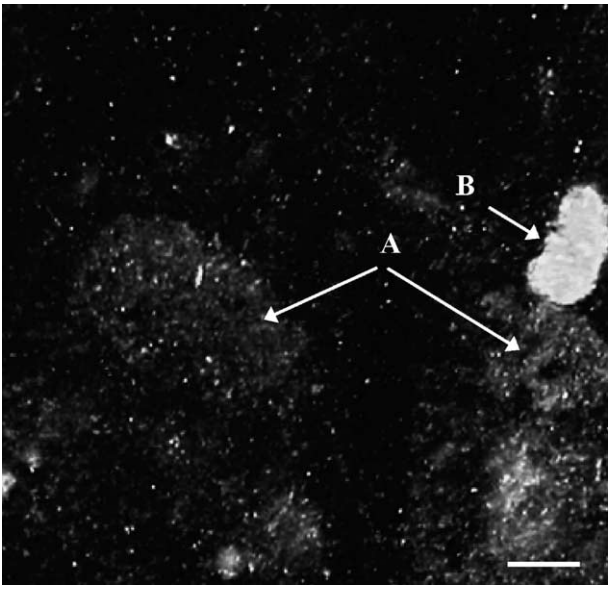

Fig. 1. Black and white reflected light micrograph (converted from color) from a ~ 0.5-mm-thick soil section prepared from the A horizon of the soil used in this study. Features labeled A (gray tone) are iron oxide aggregates. Feature labeled B (bright yellow in color turns white in black and white transformation) is an iron sulfate aggregate. Black regions are shale matrix (brown in color photo). White bar is 100 μm long.

In Fig. 2a, the comparison of the EXAFS spectrum from ferrihydrite, goethite, jarosite, and hematite standards clearly shows that there are distinct features that can be used to identify the minerals. The goethite and jarosite spectra reported by Savage et al. (2000) had similar spectral features as the spectra shown in this study. For the iron oxides, there

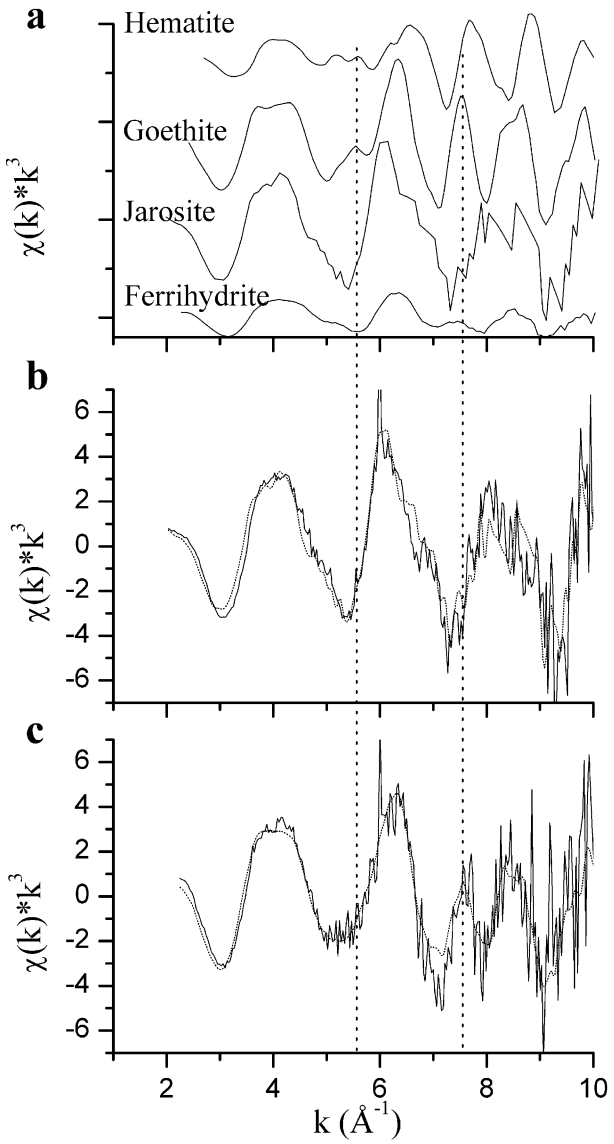

Fig. 2. EXAFS spectra from iron mineral standards and iron mineral aggregates in Fig. 1. Panel a: reference mineral spectra used to fit raw data (solid lines) in Panels b and c. Panel b: EXAFS spectrum from feature B in Fig. 1, best fit (dashed line) was obtained by using 100% jarosite standard. Panel c: EXAFS spectrum from feature A in Fig. 1, best fit was obtained by combining 74% ferrihydrite, 26% goethite.

are significant differences in the size, shape, and position of the small shoulders and peaks between 5 and 6 $Å^{-1}$, while the jarosite has a distinct difference in the phase of the chi structure after 7 $Å^{-1}$. The EXAFS spectra from the orange and yellow aggregates are shown in Fig. 2b and c together with the best fits from the linear combination of the standards. The best fit for the orange aggregate material was obtained by combining the ferrihydrite (74%) and the goethite (26%) spectra. The resulting spectra from this combination represented the data very well (Fig. 2b). An attempt to fit hematite to the spectra resulted in a very small contribution and the residual of the fit was larger than the fit with just goethite and ferrihydrite. The addition of jarosite resulted in a negative contribution when added to the fit of the orange aggregate. In the linear combination, the fit was dependent on the spectral features (i.e., wavelength and nodes or shoulders) and the amplitude of the oscillations. The amplitude of the EXAFS spectra from the iron mineral aggregates is not only affected by the degree of structural order, but also self-absorption of the fluorescence signal since they were collected in fluorescence mode. Since the standards were collected in transmission (no self-absorption), there are additional inaccuracies that are introduced into the fit results. Thus, the percent of the components that the linear composition yielded is semiquantitative and only provides a measure of relative amounts. To test the effects of amplitude on the linear combination fit results, the amplitude of the chi structure from the ferrihydrite standard was doubled and the EXAFS from the iron oxide aggregate was refit. This resulted in a decrease in the ferrihydrite contribution to 55%, verifying that there is some sensitivity of the fit results to the chi structure amplitude. However, since the fit results still yielded greater than 50% ferrihydrite, it is likely that the composition of the iron oxide aggregate has more ferrihydrite in it than goethite. The best fit of the EXAFS spectrum from the yellow aggregate was obtained by fitting only the single jarosite standard (Fig. 2c). When goethite or hematite was added to the fit of the jarosite aggregate, the result was less than 1% contribution. An attempt to use the ferrihydrite standard spectrum in the fit of the yellow aggregate resulted in a 27% ferrihydrite composition; however, the fit residual increased indicating a poorer fit than when just the jarosite standard spectrum was used. Thus, it is concluded that the yellow aggregate is composed of predominantly jarosite. The other iron oxides (lepidocrocite, maghemite, etc.) and iron sulfates (schwertmannite and natrojarosite) were not tested for; however, we expect that their concentrations are low and would be difficult to detect in these experiments.

Mermut et al. (1985) found that the mineral composition of the surface horizon of a soil formed in pyritic shale parent material located in Saskatchewan, Canada consisted of quartz, amphiboles, feldspars, and micas, with some iron oxide glaebules. From the SEM and TEM micrographs, they identified amorphous iron oxides that were clustered together with jarosite crystals in the lower horizons. Dudas et al. (1988) analyzed the minerals in a sulfate soil (pyritic shale parent material) from Alberta, Canada using differential XRD and aqueous speciation modeling based on thermodynamics. Similar to Mermut et al. (1985), they found that jarosite was common in the lower horizons but absent from the A horizon. However, they were unable to detect ferrihydrite using differential X-ray diffraction, and identified the iron oxide rich soil fractions collected from the lower horizons as goethite and hematite. Ross et al. (1988) found similar trends in the spatial distribution of jarosite in an acid sulfate soil from Manitoba, Canada. However, using the

same technique as Dudas et al. (1988), they found that ferrihydrite dominated the iron oxide mineralogy of the surface horizon, and goethite was the most common iron oxide in the lower horizons. The increased weathering in the Canadian soils is likely the reason for the lack of jarosite minerals in the surface horizon as compared to the soils from this study that are located in an arid region prone to intense erosion. The variability in the iron oxide mineralogy reported in the literature may be a result of temperature and other soil weathering and formation factors (i.e., organic matter content, soil pH, rainfall, redox, crystallization time, etc.), as well as analytical technique. The results of this study show not only the ability of EXAFS spectroscopy to distinguish iron oxide minerals, but also demonstrates the ability of μ-EXAFS spectroscopy to distinguish features that are sub-millimeter in size, and located only a few microns apart.

3.2. Microscale distribution of elements

The XRF spectra from a goethite aggregate and a jarosite aggregate are shown in Fig. 3a and b, respectively. The $K_{\alpha 1}$ peaks for As and Se are located at 10.543 and 11.222 keV, respectively. The $K_{\beta 1}$ peaks for As (11.7262 keV) and Se (12.4959 keV) could not be detected because of their low intensity and the presence of the inelastic scattering curve from the X-ray beam. The much higher intensity of the As and Se emission lines in the iron oxide aggregate (Fig. 3a) indicates that there was a higher concentration of these elements associated with the iron oxide minerals than the jarosite minerals (Fig. 3b). Other peaks are also present in the XRF spectra, such as Mn ($K_{\alpha 1} = 5.8988$ keV), Zn ($K_{\alpha 1} = 8.6389$ keV), and Ti ($K_{\alpha 1} = 4.5108$ keV). The distribution maps for these elements are not shown; however, the Mn distribution in the soil is directly correlated with the Fe distribution, the Ti distribution is correlated with Ca and Si distributions, and the Zn distribution is not correlated with any other elements in the soil section.

The spatial distributions of the elements in the thin section are shown in Fig. 4. Similar to Fig. 1, there were small orange and yellow aggregates present in the thin section analyzed in this experiment. These aggregates are indicated in Fig. 4a by the regions with high Fe concentrations. The presence of relatively high concentrations of S and K (Fig. 4b and c) in the iron aggregate centered at $x = 495$ μm and $y = 200$ μm provides elemental data to support the claim that this feature is jarosite ($KFe_3(OH)_6(SO_4)_2$). To further evaluate possible relationships, paired elemental concentrations from selected *xy* scans were plotted against each other as scatter plots (Fig. 5). Fig. 5a shows the S vs. Fe concentration. Two data fields can be identified in this figure; one shows a positive relationship between S and Fe concentrations, and the other shows little or no increase in S concentration with Fe. The positive relationship between the Fe and S concentrations is indicative of the jarosite aggregate, while the field of data that lack a correlation are indicative of the iron oxide aggregate. Similarly, at S concentrations greater than 50 μg cm^{-2}, there is a positive relationship between K and S concentrations (Fig. 5b) that is consistent with the composition of jarosite.

The distribution of As and Se shown in Fig. 4c and e indicates that these elements were more concentrated in the iron oxide aggregates than the clay/shale matrix and the jarosite aggregate. Fig. 5c and d shows that there are positive relationships between Se and As, and Fe concentrations. Fig. 5c shows at least two unique distributions of Se and Fe. One

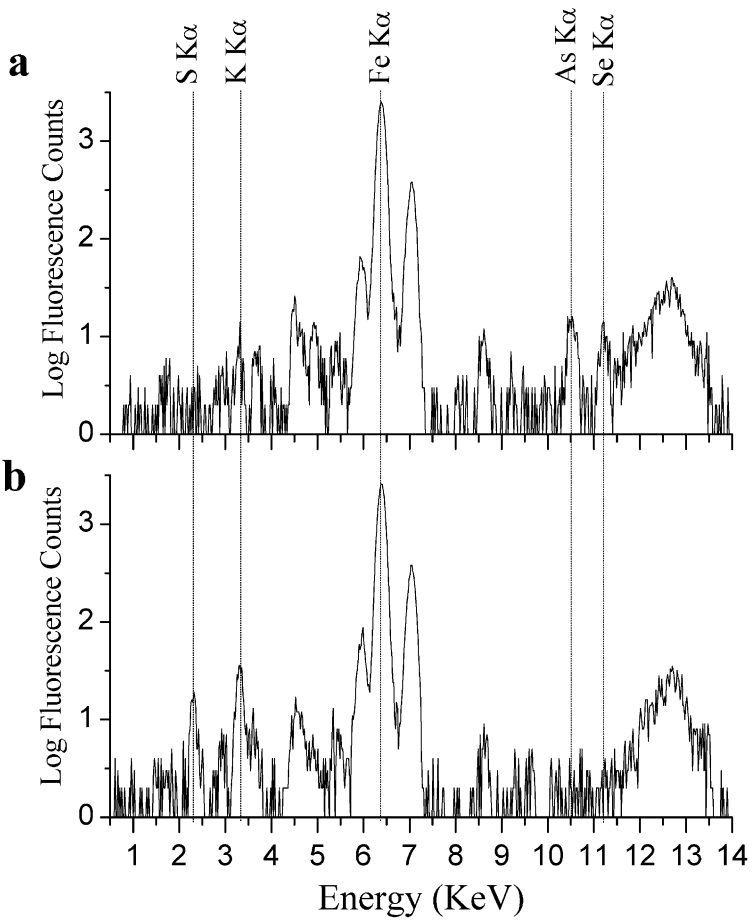

Fig. 3. XRF spectra collected from iron oxide aggregate (Panel a) and iron sulfur aggregate (Panel b) in Fig. 4.

possible explanation for this distribution is that it represents two different iron oxide aggregates. Similar trends are evident for As in Fig. 5d, although not as distinct. Using S as the indicator for jarosite, it is apparent from Fig. 5e that there was little correlation between As and Se concentrations and jarosite.

The total concentrations of As and Se in the soils were 13.7 and 6.76 mg (kg soil)$^{-1}$, respectively. Based on the results presented in this section, it appears that the As and Se were hyperaccumulated by the iron oxide minerals in the soil. Iron oxides are one of the end products of oxidative pyrite weathering. The accumulation of As and Se on these minerals suggests that either the elements coprecipitated with the iron oxide and not the jarosite, or they were sorbed much more strongly on the functional groups of the oxide than the other minerals present in the soil. Dudas et al. (1988) determined the total As concentration in mineral separates from the B and C horizons of an acid sulfate soil that formed from shale materials in a forest in Alberta, Canada. Similar to this study, they

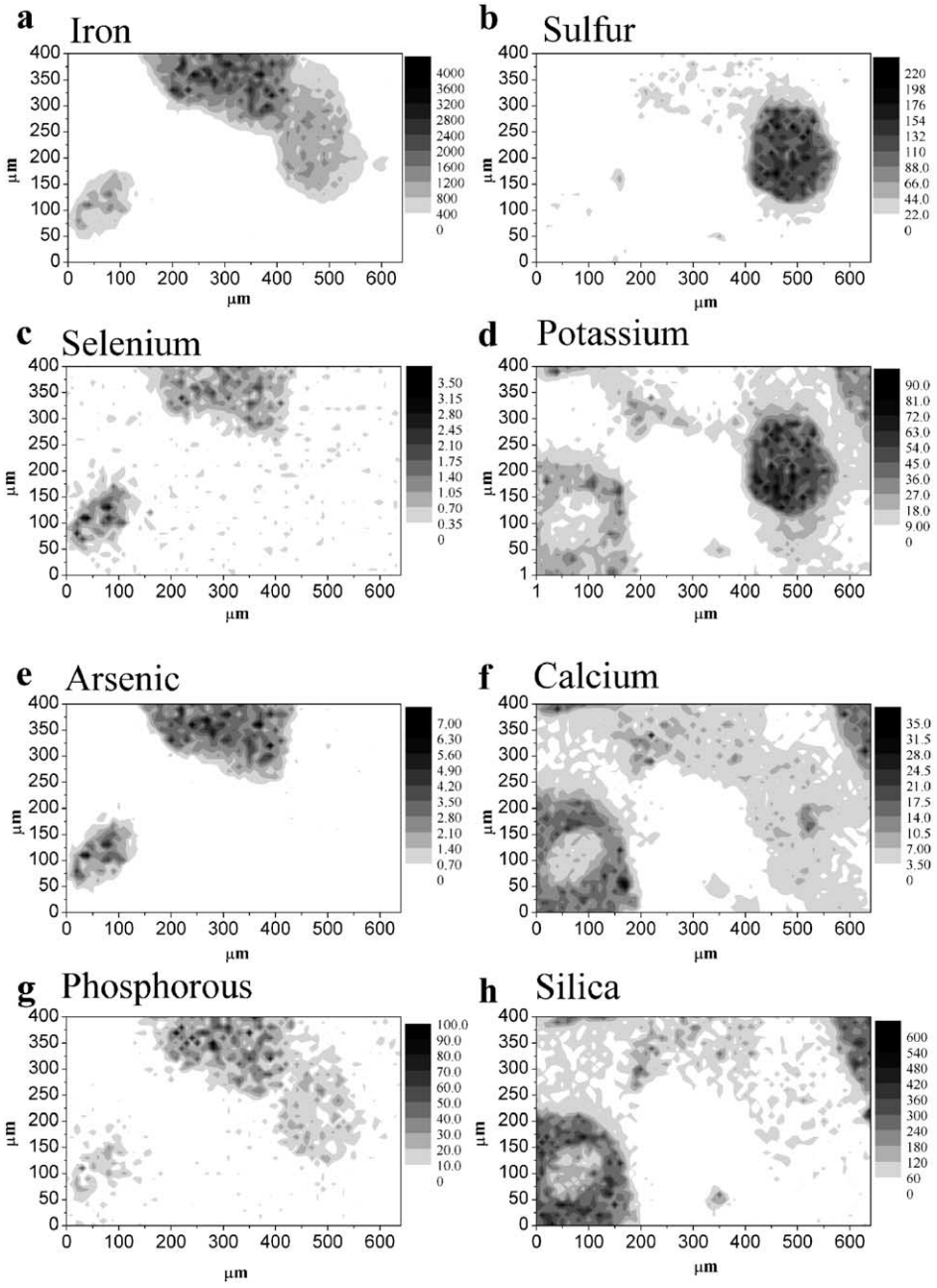

Fig. 4. Elemental distributions obtained from a 0.4 × 0.6 mm area in a ~ 3-mm-thick soil section taken from the top horizon of the soil used in this study. Concentrations are in µg/cm^2.

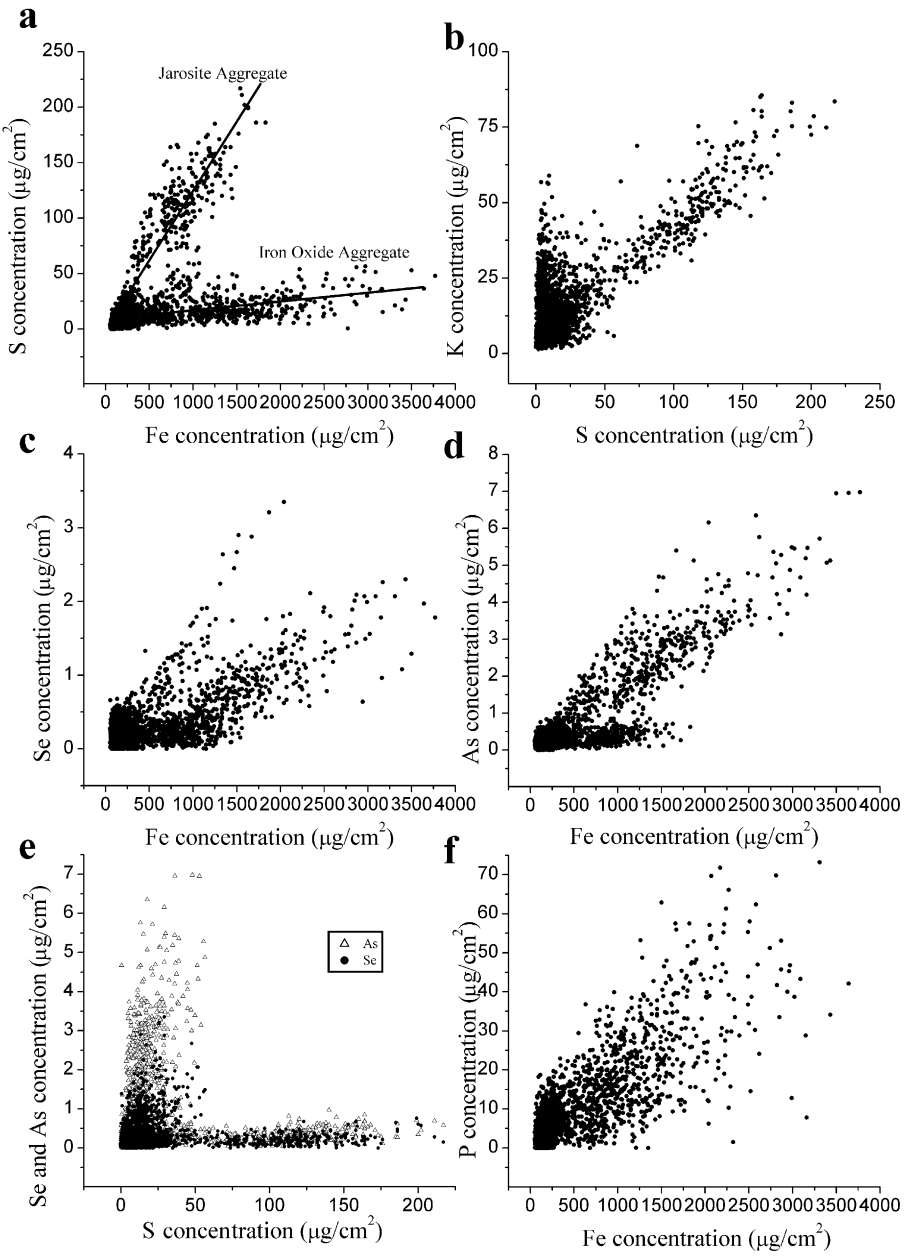

Fig. 5. Element associations for selected elements shown in Fig. 4.

found that the As was concentrated in the iron oxide fraction by 10–20 times the level in the jarosite fractions, and at least 10 times the bulk soil concentration. Foster et al. (1998) found that the predominant speciation of arsenic in weathered pyritic mine tailings was either a coprecipitated scorodite like mineral, or adsorbed on the surfaces of iron and aluminum oxides. Savage et al. (2000) reported that the arsenic in weathered pyritic mine tailings was either adsorbed on the surfaces of iron oxides, or coprecipitated with iron sulfate minerals. Our results provide direct evidence on the microscale that iron oxides preferentially accumulate As and Se over jarosite.

The elemental distribution of P is shown in Fig. 4g. The highest P concentrations were found in the jarosite and iron oxide aggregates. There was a direct relationship between the P and the Fe distribution (Fig. 5f). The total P concentration in the soil was 660 mg (kg soil)$^{-1}$. Phosphorus and As are thought to be analogous in their chemical behavior. However, in these soils, they exhibited different partitioning behavior. Phosphorus was associated with the both the iron oxide and the jarosite aggregates, while As is only associated with the iron oxide aggregates. O'Reilly et al. (2001) showed that only 35% of the sorbed arsenate could be desorbed from goethite, even though the phosphate desorptive solution was three times the concentration of the initial arsenate sorption solution. This suggests that the arsenate bond on iron oxides is stronger than the phosphate bond, and may be a reason for the dissimilar behavior of the two elements in this soil.

Calcium was distributed throughout the thin section (Fig. 4f). There was a relatively high concentration of calcium surrounding the iron oxide aggregate centered at $x = 90$ μm and $y = 100$ μm. The reason for this high Ca concentration is not clear. However, similar distributions have not been observed in other element micrographs from thin sections of the same soil. In the lower profile, Ca hot spots were identified that are correlated with S; Fig. 6 shows the elemental distribution of one of these features. Increased Ca–S concentrations were observed in regions where salt crystals are visible, and are most likely gypsum crystals, and had no accumulations of As. Mermut et al. (1985) found similar gypsum features in the lower horizon of a soil formed in Saskatchewan, Canada. Since S was not correlated with the Ca in the feature identified in Fig. 4f, it is not likely to be gypsum. Silicon, Ti, and K were also closely associated with Ca in the soil thin section (Fig. 4h). The Ca–S–K may be a weathering rind; however, it is difficult to speculate about the mineralogy and formation of this feature without additional information.

3.3. Oxidation states of As and Se in soil aggregates

The As XANES spectra are presented in Fig. 7. For determination of the effects of the resin impregnation on the As oxidation state a small soil core was spiked with As(III) and carried through the impregnation and thin sectioning steps as described above. In the As(III) spiked soil matrix and jarosite aggregates, the XANES spectra in Fig. 7b show peaks that are indicative of both As(III) and As(V), indicating that during the preparation of the thin sections, As was oxidized in these mineral aggregates (note, successive scans over time indicated no change in the spectra from photon induced oxidation). In contrast to the jarosite and soil matrix aggregates, the oxidation state of the spiked As(III) in the iron oxide aggregate shows no As(V), indicating that the As(III) oxidation state was preserved in this sample. Note that the peak from the native As(V) was masked since it was present

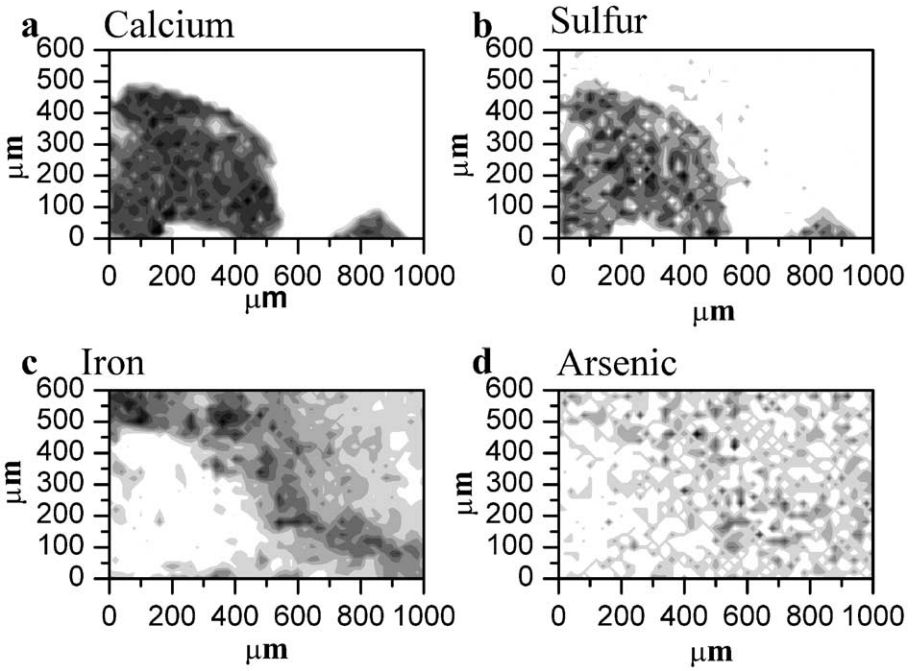

Fig. 6. Elemental distributions obtained from a 0.6 × 1 mm area in a ~ 1-mm-thick soil section taken from the horizon below 3 cm in the soil used in this study. Dark areas are the highest fluorescent counts and white areas are the lowest.

at much lower concentrations than the spiked As(III) (the concentration of native As was approximately 1/50 the concentration of spiked As(III)). These data show that the oxidation state of As on the iron oxide aggregate was preserved through the resin impregnation and thin sectioning process, i.e., resin impregnation and thin sectioning could not have caused oxidation of As(III) to As(V). In the untreated iron oxide aggregate, the halfway point for the absorption edge occurred at 11.8671 keV, directly in line with the As(V) standard. Thus, the predominant oxidation state of the As in the iron oxide aggregate was As(V), with little to no As(III) present. In the reduced iron sulfur, parent material for the soil the As likely existed as FeAsS-type coprecipitates and would have a nominal oxidation state of As^0. Through pedogenic processes, the As-pyrite minerals were oxidized and the As was either leached out of the soil as As(III) since it is more mobile than As(V), or completely oxidized and sorbed onto secondary iron oxide minerals as As(V).

The Se XANES spectra are shown in Fig. 8. To test for the effects of resin impregnation and thin sectioning on the Se oxidation state, unaltered jarosite aggregates were collected using a dissecting microscope and tweezers. Jarosite was selected because the aggregates could be isolated from the rest of the soil in significant quantities and scanned as a unique unaltered phase. The XANES spectra from the unimpregnated jarosite dust and the impregnated jarosite aggregate showed that the Se oxidation states are the same (Fig. 8).

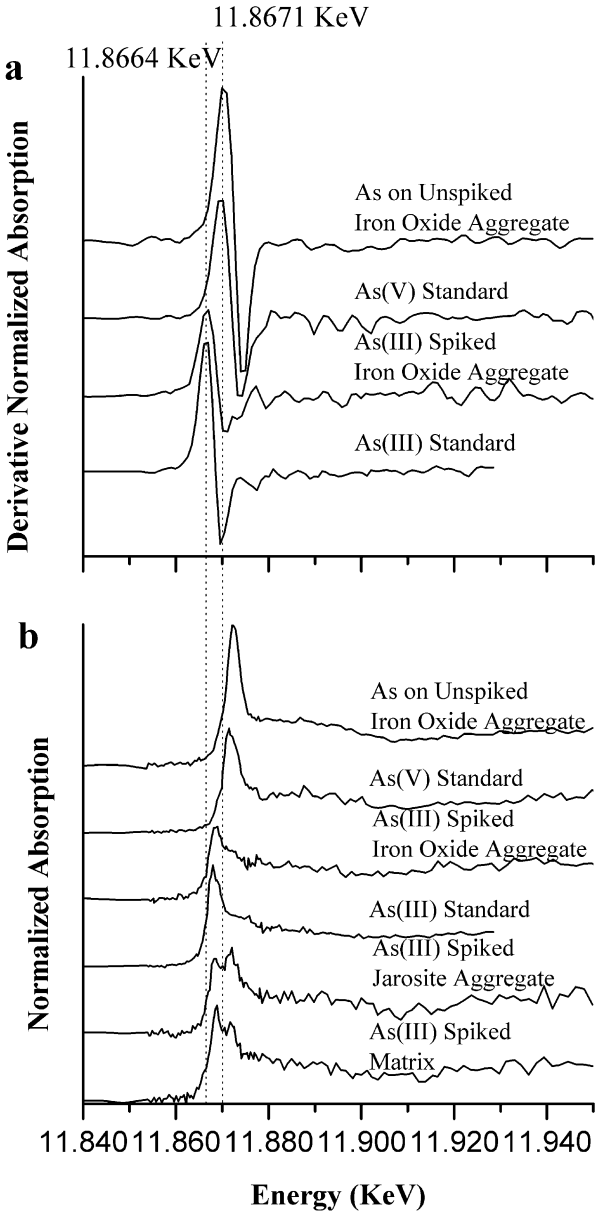

Fig. 7. Arsenic μ-XANES spectra from iron aggregates in thin section of the A horizon of soil used in this study.

This indicates that the resin impregnation process did not change the oxidation state of Se in the jarosite and most likely, not in the soil. The inflection points in the first derivative of the XANES spectra in Fig. 8a at 12.6627 and 12.6666 keV indicate that both Se(IV) and Se(VI) were present in the iron oxide and the jarosite aggregates. In the iron oxide

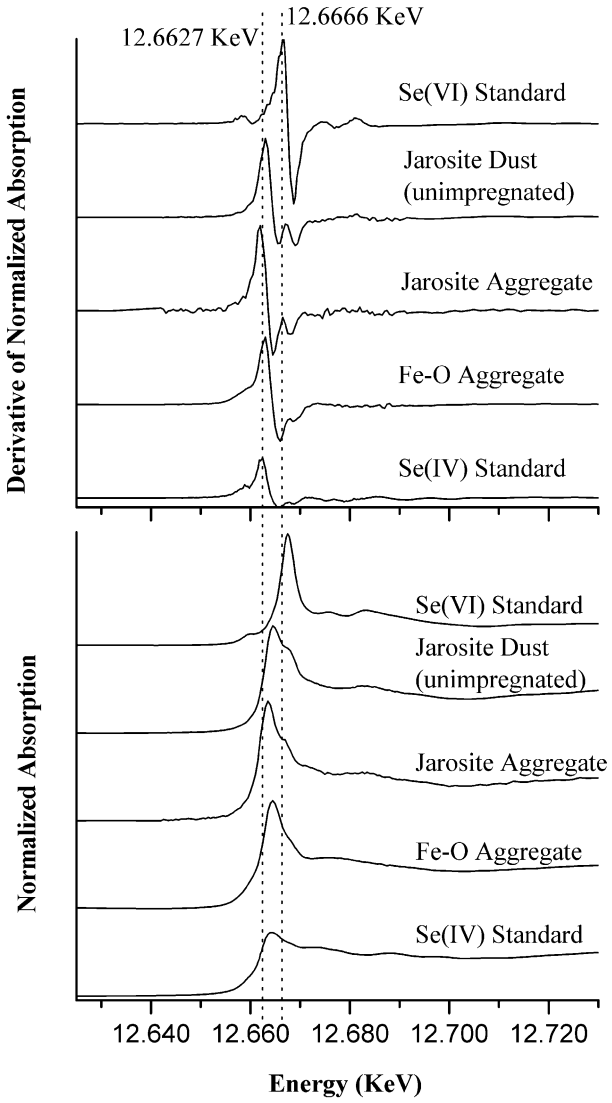

Fig. 8. Selenium μ-XANES spectra from iron aggregates in thin section of the A horizon of soil used in this study.

aggregate, the Se(VI) peak was smaller than in the jarosite aggregate, suggesting that the ratio of Se(IV) to Se(VI) was highest in the iron oxide aggregate. Selenite (Se(IV)) is known to form strong bonds and/or coprecipitates with iron oxides in soils, particularly in acid soils. In alkaline and/or oxidizing soils, selenate (Se(VI)) may also persist (McBride, 1994); however, it is less strongly adsorbed to oxides than selenite and is considered to be more mobile. Thus, since these soils are very oxidizing but have a low pH, it is likely that the selenate is coprecipitating with the jarosite minerals. The isomorphic substitution of

selenate for sulfate is favorable since the two molecules are chemical anaologues. This mechanism would account for the higher Se(VI) concentration observed in the jarosite mineral aggregate as compared to the iron oxide mineral aggregate.

4. Summary

This study presented information about the microspatial distribution of pyrite weathering products, including As, Se, P, K, S, Fe, Si, and Ca, in the top horizon of a native soil. In addition, speciation of the iron minerals and As and Se oxyanions was determined using X-ray absorption spectroscopy. We successfully determined the mineral species of two iron aggregates that were less than 100 μm in diameter and located within only a few microns of each other. One of the iron oxide aggregates was comprised of ferrihydrite and goethite and the other was predominantly jarosite. Arsenic and Se were found to be preferentially associated with the iron oxide aggregates in the soil. Selenium was present as both Se(IV) and Se(VI) oxidation states, with Se(IV) predominating. Arsenic was present only in the As(V) oxidation state. In this paper, results from only a few sections from the soil were presented. However, identical trends were observed in several sections that were scanned. Thus, the results presented in this paper are representative of the geochemical processes occurring throughout the A horizon of this soil.

The weathering of the pyrite parent materials results in the formation of secondary iron oxide and sulfate minerals. During weathering, the reduced As and Se in the pyrite are oxidized. The least mobile form of the As and Se (V and IV, respectively) remain in the soil preferentially associated with the iron oxide aggregates. The formation of iron oxide minerals in soils is dependent on several factors; of primary importance are organic matter, temperature, and pH. In these acid sulfate soils located in an arid region, the predominant iron oxide minerals observed are ferrihydrite and goethite.

The information provided by measuring the in situ oxidation states of As and Se in a naturally weathered soil formed on pyritic parent materials is important for predicting the fate and long-term geochemistry of newly exposed pyritic materials. Such information can be used to design better remediation and management strategies that will reduce the potential for environmental contamination. For example, information about the oxidation states and mineralogical associations of As and Se will allow models to be developed that will predict sorption and desorption behavior (kinetics and equilibrium) in the soil based on the true chemical speciation of the trace elements, as opposed to bulk geochemical soil properties.

Acknowledgements

We are grateful for the help in running the X-ray analysis of the samples by Gerry Lamble, Allistar MacDowell, Matt Newville, Steve Sutton, and Al Thompson. Thanks are extended to Derek Peak and Andreas Scheinost for providing the synthesized iron mineral XAFS spectra. This research was supported by the Kearney Foundation of Soil Science. Use of the Advanced Light Source was supported by the director, Office of Science, Office

of Basic Energy Sciences, U.S. Department of Energy, DE-AC03-76SF00098. GeoSoilEnviroCARS at the APS is supported by NSF EAR-9906456 (M. Rivers, PI) and DOE DE-FG02-92ER14244 and DE-FG02-94ER14466 (S. Sutton, PI). Use of the Advanced Photon Source was supported by the U.S. Department of Energy, Office of Science, Office of Basic Energy Sciences, under Contract No. W-31-109-ENG-38.

References

Alexander, M., 1995. How toxic are chemicals in soils? Environmental Science and Technology 29 (11), 2713–2717.

Bertsch, P.M., Hunter, D.B., Sutton, S.R., Bajt, S., Rivers, M.L., 1994. In situ chemical speciation of uranium in soils and sediments by micro X-ray absorption spectroscopy. Environmental Science and Technology 28, 980–984.

Dudas, M.J., Warren, C.J., Spiers, G.A., 1988. Chemistry of arsenic in acid sulphate soils of northern Alberta. Communications in Soil Science and Plant Analysis 19, 887–895.

Evangelou, V.P., Zhang, Y.L., 1995. A review: pyrite oxidation mechanisms and acid mine drainage prevention. Critical Reviews in Environmental Science and Technology 25 (2), 141–199.

Fanning, D.S., Fanning, M.C.B., 1989. Soil Morphology, Genesis, and Classification. Wiley, New York.

Fendorf, S.E., Sparks, D.L., 1996. X-ray absorption fine structure spectroscopy. In: Sparks, D.L. (Ed.), Methods of Soil Analysis. Soil Science Society of America, Madison, WI, pp. 377–416.

Fendorf, S., Eick, M.J., Grossl, P., Sparks, D.L., 1997. Arsenate and chromate retention on goethite: I. Surface structure. Environmental Science and Technology 31, 315–320.

Fennemore, G.G., Neller, W.C., Davis, A., 1998. Modeling pyrite oxidation in arid environments. Environmental Science and Technology 32, 2680–2687.

Foster, A.L., Brown Jr., G.E., Tingle, T.N., Parks, G.A., 1998. Quantitative arsenic speciation in mine tailings using X-ray absorption spectroscopy. American Mineralogist 83, 553–568.

Fuller, C.C., Davis, J.A., Waychunas, G.A., 1993. Surface chemistry of ferrihydrite: Part 2. Kinetics of arsenate adsorption and coprecipitation. Geochimica et Cosmochimica Acta 57, 2271–2282.

Gaillard, J.F., Webb, S.M., Quintana, J.P.G., 2001. Quick X-ray absorption spectroscopy for determining metal speciation in environmental samples. International Union of Crystallography 8 (2), 943–945.

Ganje, T.J., Rains, D.W., 1982. Arsenic. In: Page, A.L. (Ed.), Methods of Soil Analysis: Part 2. American Society of Agronomy, Madison, WI, USA, pp. 385–402.

Glasauer, S., Doner, H.E., Gehring, A.U., 1995. Adsorption of selenite to goethite in a flow-through reaction chamber. European Journal of Soil Science 46, 47–52.

Lumsdon, D.G., Meeussen, J.C.L., Paterson, E., Garden, L.M., Anderson, P., 2001. Use of solid phase characterisation and chemical modelling for assessing the behavior of arsenic in contaminated soils. Applied Geochemistry 16, 571–581.

MacDowell, A.A., et al., 1998. Progress toward sub-micron hard X-ray imaging using elliptically bent mirrors. Proceedings of SPIE, The International Society for Optical Engineering 3152, 126–133.

Manceau, A., Charlet, L., 1994. The mechanism of selenate adsorption on goethite and hydrous ferric oxide. Journal of Colloid and Interface Science 168, 87–93.

Manceau, A., et al., 1996. Direct determination of lead speciation in contaminated soils by EXAFS spectroscopy. Environmental Science and Technology 30 (5), 1540–1552.

Manceau, A., et al., 2000. Quantitative Zn speciation in smelter-contaminated soils by EXAFS spectroscopy. American Journal of Science 300, 289–343.

Manning, B., Goldberg, S., 1997. Adsorption and stability of arsenic(III) at the clay mineral–water interface. Environmental Science and Technology 31, 2005–2011.

Manning, B.A., Fendorf, S.E., Goldberg, S., 1998. Surface structures and stability of arsenic (III) on goethite: spectroscopic evidence for inner-sphere complexes. Environmental Science and Technology 32, 2383–2388.

Masschelyn, P.H., Delaune, R.D., Patrick Jr., W.H., 1991. Biogeochemical behavior of selenium in anoxic soils and sediments: an equilibrium thermodynamics approach. Journal of Environmental Science and Health A26, 555–573.

McBride, M.M., 1994. Environmental Chemistry of Soils. Oxford Univ. Press, New York, NY, 406 pp.
McSweeney, K., Madison, F.W., 1988. Formation of a cemented subsurface horizon in sulfidic minewaste. Journal of Environmental Quality 17, 256–262.
Mermut, A.R., Curtin, D., Rostad, H.P.W., 1985. Micromorphological and submicroscopical features related to pyrite oxidation in a inland marine shale from east central Saskatchewan. Soil Science Society of America 49, 256–261.
National Cooperative Soil Survey, 1997. Official Soil Series Descriptions. Soil Survey Division, Natural Resources Conservation Service, United States Department of Agriculture.
Nesbitt, H.W., Muir, I.J., Pratt, A.R., 1995. Oxidation of arsenopyrite by air and air-saturated, distilled water, and implications for mechanism of oxidation. Geochimica et Cosmochimica Acta 59, 1773.
O'Reilly, S.E., Strawn, D.G., Sparks, D.L., 2001. Residence time effects on arsenate adsorption/desorption mechanisms on goethite. Soil Science Society of America 1, 67–77.
Presser, T.S., Ohlendorf, H.M., 1987. Biogeochemical cycling of selenium in the San Joaquin Valley, California, USA. Environmental Management 11, 805–821.
Presser, T.S., Swain, W.C., 1990. Geochemical evidence for Se mobilization by the weathering of pyritic shale, San Joaquin Valley, California, U.S.A. Applied Geochemistry 5, 703–717.
Raven, K.P., Jain, A., Loeppert, R.H., 1998. Arsenite and arsenate adsorption on ferrihydrite: kinetics, and adsorption envelopes. Environmental Science and Technology 32, 344–349.
Ribet, I., Ptacek, C.J., Blowes, D.W., Jambor, J.L., 1994. The potential for metal release by reductive dissolution of weathered mine tailings. Journal of Contaminant Hydrology 17, 239–273.
Ross, G.J., Eilers, R.G., Ivarson, K.C., 1988. Influence of acid sulfate weathering on chemical and mineralogical properties of an acid sulfate soil of Manitoba. Canadian Journal of Soil Science 68, 629–644.
Savage, K.S., Tingle, T.N., O'Day, P.A., Waychunas, G.A., Bird, D.K., 2000. Arsenic speciation in pyrite and secondary weathering phases, Mother Lode District, Toulumne County, California. Applied Geochemistry 15, 1219–1244.
Scheinost, A.C., Schwertman, U., 1999. Color identification of iron oxides and hydroxysulfates: use and limitations. Soil Science Society of America Journal 63, 1463–1471.
Schwertmann, U., Taylor, R.M., 1989. Iron oxides. In: Dixon, J.B., Weed, S.B. (Eds.), Minerals in the Soil Environment. Soil Science Society of America, Madison, pp. 379–427.
Sencindiver, J.C., Ammons, J.T., 2000. Minesoil genesis and classification. In: Barnhisel, R.I., Darmody, R.G., Daniels, W.L. (Eds.), Reclamation of Drastically Disturbed Lands. Agronomy Monograph. American Society of Agronomy, Madison.
Sposito, G., DeWit, J.C.M., Neal, R.H., 1988. Selenite adsorption on alluvial soils: III. Chemical modeling. Soil Science Society of America 52 (4), 947–950.
Sun, X., Doner, H.E., 1998. Adsorption and oxidation of arsenite on goethite. Soil Science 163, 278–287.
Tamaki, S., Frankenberger, W.T., 1992. Environmental biochemistry of arsenic. Reviews of Environmental Contamination and Toxicology 124, 79–110.
Tokunaga, T.K., Brown, G.E., Pickering, I.J., Sutton, S.R., Bajt, S., 1997. Selenium redox reactions and transport between ponded waters and sediments. Environmental Science and Technology 31, 1419–1425.
Tokunaga, T.K., Sutton, S.R., Bait, S., Nuessle, P., Shea-McCarthy, G., 1998. Selenium diffusion and reduction at the water sediment boundary: micro-XANES spectroscopy of reactive transport. Environmental Science and Technology 32, 1092–1098.
Velinsky, D.J., Cutter, G.A., 1990. Determination of elemental selenium and pyrite-selenium in sediments. Analytica Chimica Acta 235, 419–425.
Zavarin, M., 1999. Sorptive properties of synthetic and soil carbonates for selenium, nickel, and manganese. PhD Thesis, University of California-Berkeley, Berkeley, CA, 279 pp.
Zhang, Y., Moore, J.N., Frankenberger, W.T., 1999. Speciation of soluble selenium in agricultural waters and aqueous soil-sediment extracts using hydride generation atomic absorption spectrometry. Environmental Science and Technology 33, 1652–1656.